# Pressure-Induced Conductivity in a Neutral Nonplanar Spin-Localized Radical

Manuel Souto,[†] HengBo Cui,[‡] Miriam Peña-Álvarez,[§] Valentín G. Baonza,[§] Harald O. Jeschke,[∥] Milan Tomic,[∥] Roser Valentí,[∥] Davide Blasi,[†] Imma Ratera,[†] Concepció Rovira,[†] and Jaume Veciana*,[†]

[†]Institut de Ciència de Materials de Barcelona (ICMAB-CSIC)/CIBER-BBN, Campus Universitari de Bellaterra, 08193 Cerdanyola del Vallès (Barcelona), Spain
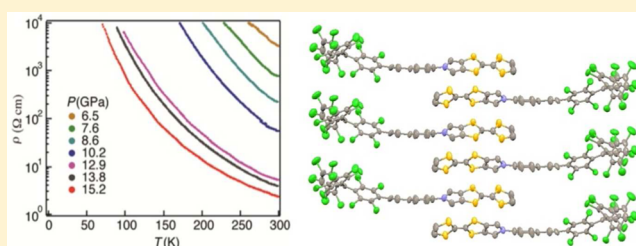
[‡]Condensed Molecular Materials Laboratory, RIKEN, Wako-shi, Saitama 351-0198, Japan

[§]MALTA CONSOLIDER Team, Departamento de Química Física I, Facultad de Ciencias Químicas, Universidad Complutense de Madrid, 28040 Madrid, Spain

[∥]Institut für Theoretische Physik, Goethe-Universität Frankfurt, Max-von-Laue-Straße 1, 60438 Frankfurt am Main, Germany

**S** *Supporting Information*

**ABSTRACT:** There is a growing interest in the development of single-component molecular conductors based on neutral organic radicals that are mainly formed by delocalized planar radicals, such as phenalenyl or thiazolyl radicals. However, there are no examples of systems based on nonplanar and spin-localized C-centered radicals exhibiting electrical conductivity due to their large Coulomb energy ($U$) repulsion and narrow electronic bandwidth ($W$) that give rise to a Mott insulator behavior. Here we present a new type of nonplanar neutral radical conductor attained by linking a tetrathiafulvalene (TTF) donor unit to a neutral polychlorotriphenylmethyl radical (PTM) with the important feature that the TTF unit enhances the overlap between the radical molecules as a consequence of short intermolecular S···S interactions. This system becomes semiconducting upon the application of high pressure thanks to increased electronic bandwidth and charge reorganization opening the way to develop a new family of neutral radical conductors.

## INTRODUCTION

In the last decades, there has been a huge development of molecular conducting materials based on two components, one of which is a $\pi$-extended organic acceptor (or donor) molecule. Such a compositional characteristic is motivated by the need to generate charge carriers in the solid material, which is achieved either by a charge transfer (CT) between the donor and acceptor components, if both are present, or by a partial doping of such $\pi$-extended molecules with an extrinsic redox agent. These systems should have an additional prerequisite for exhibiting electrical conductivity, namely an appropriate packing of the doped molecules that permits the overlap between the frontier orbitals of neighboring molecules along one, two, or even three dimensions of the material.[1−3] More recently, single-component molecular conductors have been developed based on planar metal bis-dithiolene complexes, which exhibit structural and electronic characteristics that combine the presence of charge carriers and a proper molecular packing.[4,5] The soft nature of all these molecular crystals permits to tune their electronic properties by applying pressure, which allows to switch from a semiconductor material to a metal or even a superconductor.[6,7]

In view of the importance of obtaining crystals of single-component molecular conductors, the use of neutral organic radicals as building blocks for molecular conductors has

appeared as alternative due to the possibility that the unpaired electrons can serve as charge carriers without the need of a previous doping process.[8] Phenalenyl-based radicals, developed by Haddon,[9−17] and thiazolyl-based radicals, by Oakley,[18−22] are good examples of such materials. The solid state electronic structure of this kind of crystals is best described in terms of the half-filled band ($f = 1/2$) Mott−Hubbard model, with one electron associated with each radical site. One of the keys to attain conductivity in these single-component radical-based materials and overcome the charge repulsion problem is to maximize the electronic bandwidth $W$ ($= 4\beta$) ($\beta =$ intermolecular resonance integral) and minimize the intrasite Coulomb repulsion energy $U$. When the electronic bandwidth is sufficient to offset charge repulsion ($W > U$), conductivity would take place.[20] Synthetic strategies to produce conductive radical-based materials have focused on the use of highly delocalized planar organic systems, which have the benefit of a low value of $U$, and the incorporation of heavy (soft) heteroatoms in these structures, which can lead to an enhanced bandwidth $W$.[21] However, there are no reported examples of single-component molecular conductors based on nonplanar and spin-localized carbon-centered organic radicals due to their

weak electronic intermolecular interactions leading to narrow electronic bandwidth and their large intrasite electronic repulsion. Finding new ways to overcome this shortage could expand the possibilities to generate novel single-component molecular conductors.

Organic molecules containing electron donor (D) and electron acceptor (A) units linked by π-conjugated bridging groups are worthy of attention for the investigation of intramolecular electron transfer phenomena and its associated bistability event.[23] Recently, we have reported a D−A dyad based on a tetrathiafulvalene (TTF), an electron π-donor, connected to a polychlorotriphenylmethyl (PTM) radical, a good electron acceptor, which exhibits bistability in solution through the application of external stimuli such as the polarity of the solvent or temperature.[24−26] Indeed, molecules of this D−A dyad coexist in two electronic structures, one neutral and another zwitterionic, due to the intramolecular charge transfer process between the D and A subunits. Therefore, such a kind of radical D−A dyads are promising candidates to show novel physics when moving from solution to solid state if one takes advantage of the intramolecular CT to generate a doping in the subunits. In order to exploit the physical properties in solid state such as conductivity and magnetism of this kind of species, we have recently obtained the radical donor−acceptor dyad 1 (MPTTF-PTM), based on a PTM radical unit linked to a monopyrrolotetrathiafulvalene (MPTTF) unit through a π-conjugated phenyl-vinylene bridge (Figure 1). The bridge was
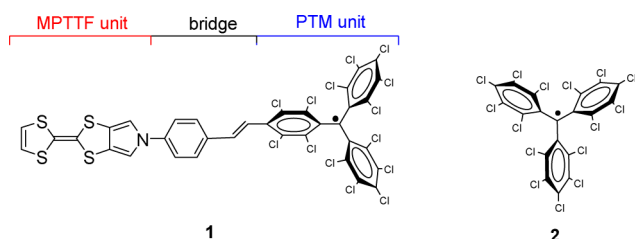


**Figure 1.** Chemical structures of the neutral radical dyad MPTTF-PTM (**1**) and perchlorotriphenylmethyl (PTM) radical (**2**).

added in order to decrease the steric repulsion between the PTM radical units and to take advantage of the TTF subunit to pack forming chains. Indeed, this system shows a supramolecular architecture with segregated donor and acceptor units where the TTF units are arranged forming herringbone-type 1-D chains and a close packing of the PTM units.[27]

In this work and in accordance with the intrinsic softness of molecular crystals we report the appearance of conductivity in single crystals of radical dyad **1** induced by pressure in contrast to the Mott insulator behavior of the unsubstituted perchlorotriphenylmethyl radical **2** under all applied pressures. Thus, the conductivity in **1** with pressure is related to the enhancement of the intermolecular overlap between the MPTTF-PTM molecules due to incorporation of TTF units. This forces the formation of closed packed stacks of molecules and, thus, the increase of W. Band structure calculations based on density functional theory (DFT) on ab initio-predicted MPTTF-PTM crystal structures under pressure confirm the significant increase of W in radical dyad **1** as a function of pressure. These calculations suggest important modifications on the electronic structure at pressures above 6−8 GPa with an increase in charge delocalization and of the W/U ratio. These effects are clearly observed in our combined analysis of Raman

and DFT calculations under pressure. Moreover, high-pressure Raman and photoluminescence spectroscopy show important conformational changes that could indicate a change of the crystalline phase when the system is compressed at very high pressures. Up to our knowledge, this is the first example of a single-component molecular conductor based on a nonplanar and C-centered neutral radical with highly localized spins that exhibits a semiconductor behavior with high conductivity and low activation energy.

## ■ RESULTS

**Crystallography.** X-ray diffraction analysis on red crystals of radical **2**, obtained by a slow diffusion in a mixture of dichloromethane/hexane (1:1) at room temperature, reveals a new polymorph of PTM radical that crystallizes in the triclinic system with a $P\bar{1}$ space group and the asymmetric unit is formed by two equivalent molecules (Table S1 and Figure S1 in the Supporting Information). Molecules of **2** are arranged on the ab plane as shown in Figure 2 forming regular chains of
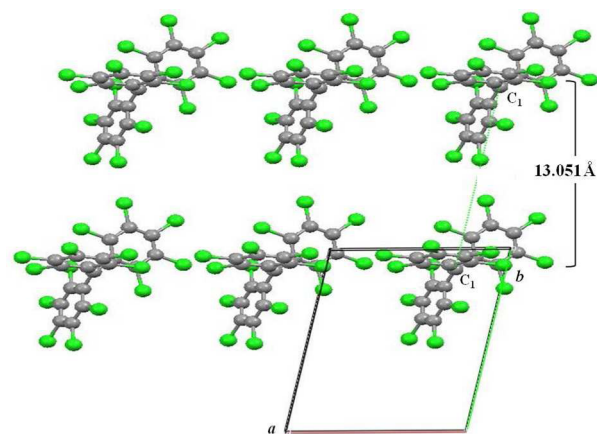


**Figure 2.** Crystal packing of radical **2** on the ab plane. The gray and green ellipsoids represent the carbon and chlorine atoms, respectively. Atoms are shown at the 50% probability level. Intermolecular distance between the central ipso-carbons of two adjacent molecules in the ab plane (C1⋯C1′) is 13 Å.

radicals connected by short Cl⋯Cl contacts. The distance between the central ipso-C (C₁) atoms of two adjacent molecules of PTM radical is 13 Å along the b-axis. Moreover, molecules are disposed on the bc plane as shown in Figure S2 showing the formation of dimers with a short contact between the phenyl rings (4.3 Å) that are oriented in a parallel position showing a distance between their central ipso-carbon (C₁) atoms of 10 Å.

On the other hand, dark crystals of radical dyad **1** were also obtained by a slow evaporation in dichloromethane/hexane at room temperature and their X-ray diffraction analysis shows a P2₁ space group with Z = 4 (Table S1 and Figure S3).[27] The asymmetric unit shows two inequivalent molecules that are chemically equivalent and exhibit a very similar geometry. Regarding the molecular arrangement, molecules of radical dyad **1** are stacked forming regular 1D chains on the ab plane in which MPTTF units are forming a herringbone structure along the b-axis with short S⋯S and Cl⋯Cl distances of 3.9 and 3.3 Å, respectively (Figure 3). Along this axis direction, the distance between the central ipso-carbon (C₁) atoms of the PTM subunit of two adjacent molecules is 7.9 Å and the planes
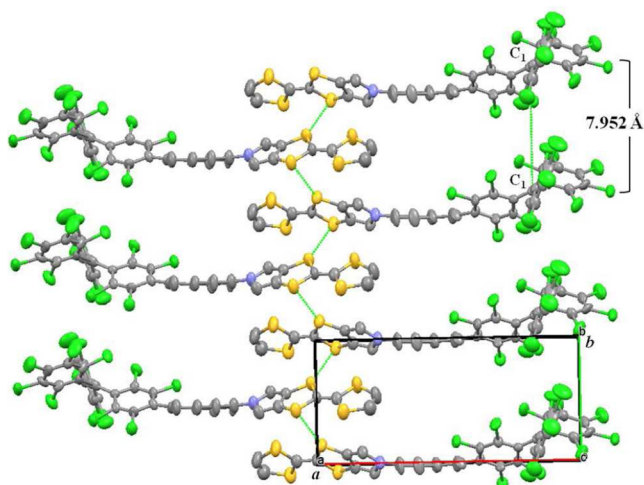
**Figure 3.** Crystal packing of radical dyad **1** on the *ab* plane showing the intermolecular distance between the central $C(1)\cdots C(1)'$ atoms (7.9 Å) of adjacent PTM molecules and short $S\cdots S$ interactions. The gray, green, blue and yellow ellipsoids represent the carbon, chlorine, nitrogen and sulfur atoms, respectively. Atoms are shown at the 50% probability level. Hydrogen atoms have been omitted for clarity.

formed by the phenyl rings of the PTM units of adjacent molecules are also oriented in a parallel fashion indicating the formation of $\pi$-type interactions between the neighboring radical units (Figure S4). Thus, the decrease of intermolecular distances between the molecular units clearly denotes a higher overlap of PTM radical units in dyad **1** in comparison with radical **2** thanks to the supramolecular self-assembly of the TTF units.

**High-Pressure Conductivity.** Resistivity measurements on crystals of **1** and **2** were performed under high pressure conditions. Three independent crystals of radical **2** were measured up to 21.2 GPa and they were found always insulating under all assayed conditions. Pressure and temperature dependence measurements of the resistivity of radical dyad **1** were also performed with three independent crystals along the *b*-axis (Figures 4, S7 and S8). Crystals of **1** showed insulating behavior at ambient pressure while increasing the pressure the room-temperature resistivity rapidly decreased exhibiting a semiconducting behavior throughout the studied temperature range. From 6.5 GPa the room-temperature resistivity linearly decreased with a negative slope of ca. 2.4 $\Omega$ cm/GPa and the conductivity at 15.2 GPa and 298 K was
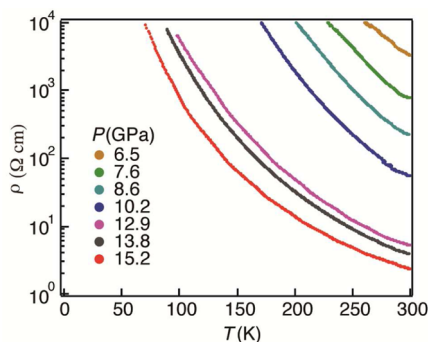


**Figure 4.** Electrical resistivity of radical dyad **1**. Temperature dependence of the resistivity of radical dyad **1** along the *b*-axis at different pressures.

found to be as high as 0.76 S cm$^{-1}$ with a low activation energy ($E_a$) of 0.067 eV ($E_a$ = 0.21 eV at $P$ = 6.5 GPa). At higher pressures the room temperature conductivity slightly decreased on increasing the pressure (see Figures S7 and S8) and the conductivity at 21.2 GPa (298 K) was 0.43 S cm$^{-1}$ with and activation energy $E_a$ of 0.073 eV. Reproducibility of measurements was confirmed using three different samples as shown in Figure S8.

**Magnetic Susceptibility.** The temperature dependence of the magnetic susceptibility ($\chi$) for a polycrystalline sample at ambient pressure of radical dyad **1** was measured over the temperature range of 2−300 K (Figure S10). The compound shows a Curie−Weiss behavior and the experimental data was fitted to obtain a Curie constant C = 0.394 cm$^3$ K mol$^{-1}$ with a $\chi_m T$ at room temperature that fully agrees with the theoretical value of 0.375 expected for noninteracting S = 1/2 systems. Upon cooling, $\chi_m T$ decreases according with the presence of weak antiferromagnetic interactions among the radical units (Weiss constant of $\theta$ = −1.06 K).

**Electrochemical Properties.** The electrochemistry of radicals **1** and **2** were examined by cyclic voltammetry (Figure S11, Table 1) in order to have an estimation of the disproportionation potential ($E_{disp}$) in solution. This value can be determined from the difference between the first oxidation and reduction potentials in solution $\Delta E_{2-1} = (E^{ox1}_{1/2} - E^{red}_{1/2})$ and provide indirect measurements of the intrasite Coulomb repulsion energy, $U$, which are usually low in highly delocalized spin systems.[17] $E^{red}_{1/2}$ electrochemical reduction corresponds to the reduction of the radical to the anion and $E^{ox1}_{1/2}$ is attributed to the first oxidation process of the molecule. In the case of radical dyad **1**, the first oxidation process is attributed to the oxidation of the electroactive TTF unit. Thus, the estimated disproportionation potentials for **1** and **2** are 0.64 and 1.80 V, respectively, confirming that the Coulomb repulsion energy $U$ is much lower for radical dyad **1**.

**Crystal Structures, Band Structure and Charge Transfer Calculations as a Function of Pressure.** In order to elucidate the microscopic origin of the pressure dependence of the electrical conductivity in radical dyad **1** and due to the absence of good quality powder X-ray diffraction data for crystal structure determination at finite pressures we decided to calculate by ab initio optimization routines the crystalline and electronic band structures at the studied pressures.

Thus, we relaxed a set of crystal structures at different pressures within density functional theory (DFT) using the projector augmented wave basis as implemented in the Vienna ab initio simulation package (VASP)[28,29] and the generalized gradient approximation (GGA)[30] (see Experimental Section and Supporting Information for details). The electronic structure and charge transfer of this series of predicted crystal structures were determined with the full potential local orbital (FPLO) basis set.[31] Figure 5 shows the evolution of lattice parameters, monoclinic angle and volume of the predicted structures as a function of pressure. While along the *a* and *b* directions the structures experience a monotonic contraction, this is not the case along the *c* direction (perpendicular to the molecular stacking) where a slight expansion at low pressures followed by a contraction at higher pressures is observed. The decrease of the monoclinic angle indicates a reduction of the structural anisotropy and we observe an enhanced planarity of the molecules at high pressures. Further below we show that our Raman analysis at high pressures is consistent with the predicted structures.

## Table 1. Electrochemical Data of Radicals 1 and 2[a,b]

| compound | $E^{red}_{1/2}$ | $E^{ox1}_{1/2}$ | $E^{ox2}_{1/2}$ | $E^{ox3}_{1/2}$ | $E_{disp}$[c] |
|---|---|---|---|---|---|
| 1 | −0.19 (PTM) | 0.45 (TTF) | 0.95 (TTF) | 1.52 (PTM) | 0.64 |
| 2 | −0.19 (PTM) | 1.61 (PTM) | − | − | 1.80 |

[a]In Volts vs Ag/AgCl; $CH_2Cl_2$ as solvent and $TBAPF_6$ as electrolyte and scan rate of 0.1 V/s. [b]In parenthesis is the subunit responsible of the redox wave. [c]$E_{disp}$ estimated as $E^{ox1}_{1/2} − E^{red}_{1/2}$.
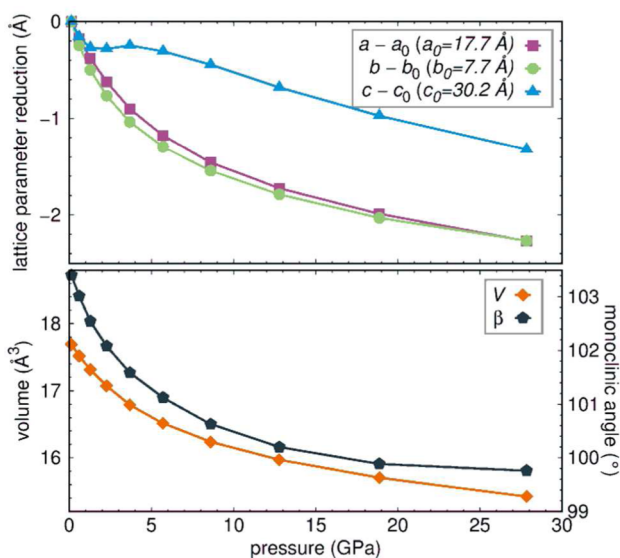


**Figure 5.** Crystal structure parameters at high pressure. Evolution of lattice parameters, monoclinic angle and volume of the predicted structures of radical dyad **1** as a function of pressure.



**Figure 6.** Electronic band structures and density of states of radical dyad **1**. The two-dimensional energy dispersion near the Fermi level at (a) ambient pressure ($P = 0$) and (b) $P = 8.6$ GPa. Path in the Brillouin Zone: X = (1/2,0,0), U = (1/2,0,1/2), R = (1/2,1/2,1/2), T = (1/2,1/2,0), Y = (0,1/2,0), V = (0,1/2,1/2) and Z = (0,0,1/2).

We analyze in what follows the electronic structure of radical dyad **1** under pressure. Figure 6 shows the GGA electronic bandstructure of the ambient pressure ($P = 0$) and the $P = 8.6$ GPa structures. At $P = 0$ the system is a Mott insulator, however as it is well-known[32] DFT in the GGA approximation is not able to reproduce this insulating state (Figure 6a) due to the insufficient treatment of electronic correlations in GGA. Albeit the absence of a gap at $P = 0$, we can still extract valuable information out of the GGA calculations. There are four half-filled narrow bands at the Fermi level arising from the four molecules per unit cell of **1** (Figure 3). PTM+bridge is contributing the majority of the carriers in the valence band with some participation of MPTTF. At higher binding energies the bands are mostly of MPTTF character with some hybridization to the PTM+bridge. The lack of dispersion along $k_z$ indicates that this system is electronically dominantly two-dimensional at ambient pressure. Upon increasing pressure (Figure 6b and S14) the bandwidth $W$ significantly increases due to enhanced intermolecular overlap and hybridizations and the system becomes more three-dimensional. This increase in $W$ and molecular hybridizations contributes to the increase of the ratio $W/U$ and the appearance of enhanced conductivity at high pressures as observed in our measurements. At 0 GPa the bandwidth of all four bands at the Fermi level is very narrow (<0.04 eV). However, with pressurization at 8.6 GPa, we observe that the gap in the valence states at −0.05 eV between the bands dominated by TTF orbitals and the bands dominated by PTM orbitals disappears and a wide band manifold of about 0.4 eV forms which is of the same magnitude as the Coulomb barrier estimated from the electrochemical data in solution.
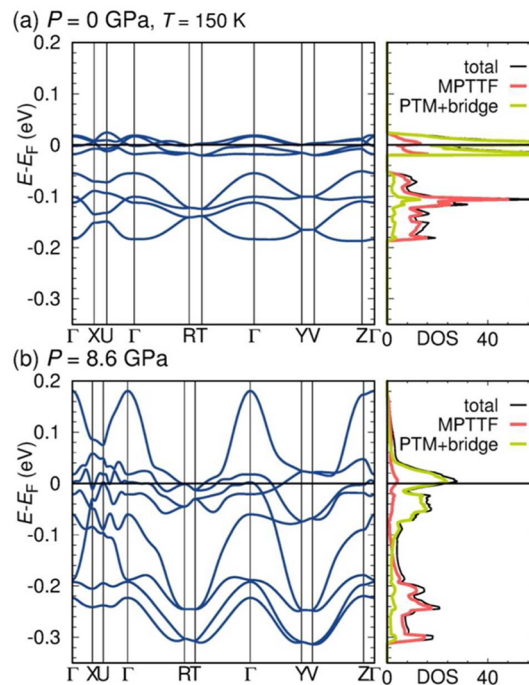
Further compression to 18.9 GPa gives rise to a higher broadening of the bands with bandwidth near 0.8 eV.

Wannier functions at ambient pressure and $P = 12.8$ GPa are shown in Figures S15 and S16 for visualizing the orbitals corresponding to the bands with dominant PTM character at the Fermi level ($E_F$) and the bands with dominant MPTTF character right below $E_F$. Under high pressure (Figure S15), the Wannier functions acquire tails on neighboring molecules; i.e., tails on PTM in the case of the SUMO, and on neighboring MPTTF and the bridge in the case of the HOMO (dark blue patches result from cuts due to unit cell boundaries).

To better understand this magnetic system, we have also performed spin-polarized GGA calculations. Figure 7a shows the spin distribution in the radical dyad **1** at $P = 0$ GPa. We observe a strong spin localization on the central C atom of the PTM units and a less pronounced spin occupation on the MPTTF units. Pressure only slightly influences the spin density distribution between the two components of the molecule as it can be seen from the evolution of the magnetic moment and spin density with pressure (Figures S28 and S29). The spin polarized bands show a gap at $P = 0$ GPa (Figure 7b) that diminishes and closes at $P > 6$ GPa (Figure 7c). Even though we do not have an advanced description of correlations as mentioned above, with the incorporation of magnetism we can track the evolution under pressure of the insulating to
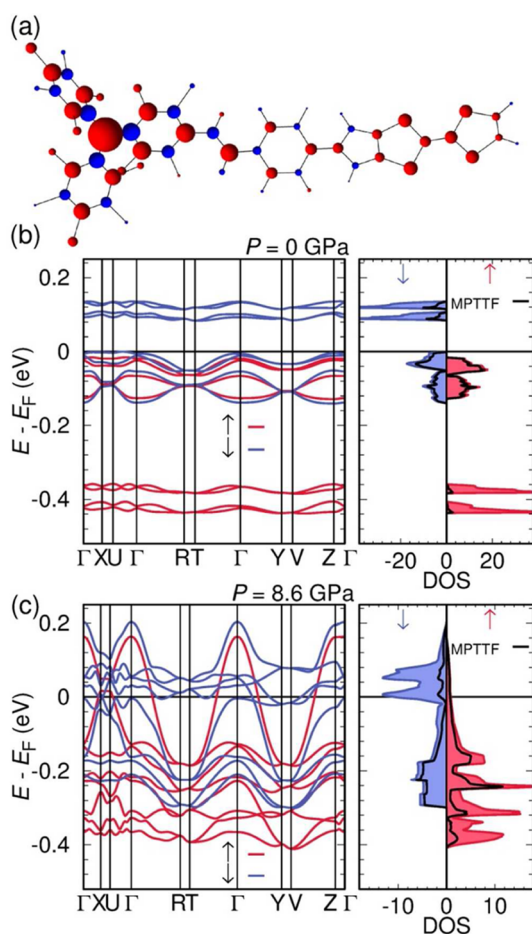
**Figure 7.** (a) Spin distribution in radical dyad **1** at 0 GPa. Spin polarized electronic band structures and density of states of radical dyad **1** at (b) 0 GPa and (c) 8.6 GPa.
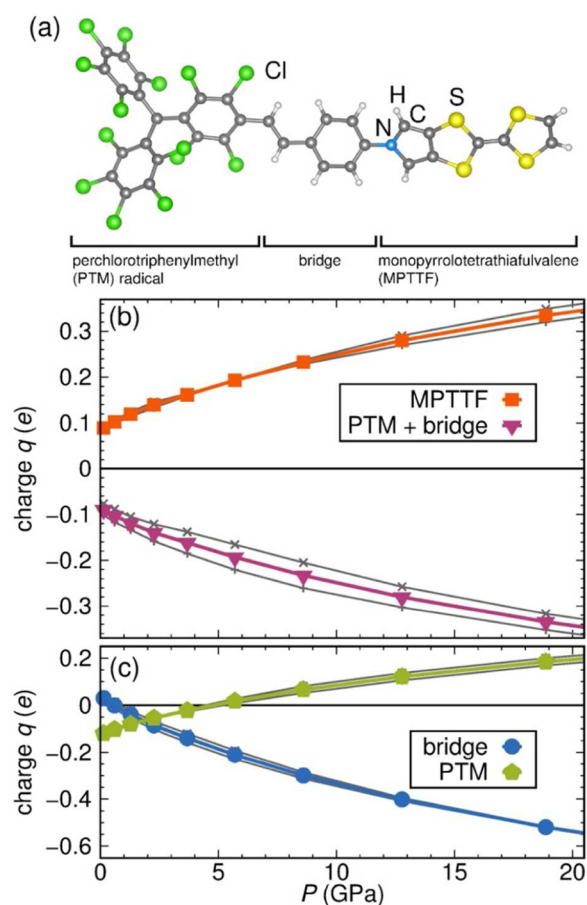


**Figure 8.** Calculated evolution of excess charge within the units of radical dyad **1** with hydrostatic pressure. (a) The different selected parts of the radical dyad **1**. (b) Excess of charge on the different units under high pressure. (c) Excess of charge on the PTM and bridge units under high pressure. The gray lines denote the excess charge corresponding to the two nonequivalent molecules of **1** under pressure.

semiconducting/metallic behavior associated with magnetism. We observe a closing of the gap between the (spin-polarized) occupied bands with dominant MPTTF character and the empty bands with dominant PTM character. An improved description of correlations—which is beyond the scope of the present study—would shift the closing of the gap to higher pressures as observed experimentally.

The pressure evolution of the charge transfer in the radical dyad **1** is displayed in Figure 8. We chose to distinguish the PTM together with the phenyl-vinylene bridge as the acceptor unit and the MPTTF as donor unit (Figure 8a). We observe (Figure 8b) that increasing the pressure, the charge transfer between the two units increases from $0.09e^-$ at ambient pressure to $0.32e^-$ at $P = 18$ GPa. In order to analyze the pressure dependence of the charge distribution in the PTM+bridge region, we plot in Figure 8c the excess charge on PTM and bridge units. We find that increasing the pressure, the PTM unit decreases in excess of charge indicating a possible electron delocalization through the bridge that is in agreement with the enhanced planarity of the system observed in the simulated crystal structures at high pressures. The charge on the donor MPTTF unit increases from $0.09e^-$ at ambient pressure to $0.25e^-$ at $P = 10$ GPa (Figure 8b). Meanwhile, the bridge which is only donating $0.03e^-$ at ambient pressure turns into an acceptor with $0.32e^-$ extra electrons at $P = 10$ GPa. This indicates that there is a charge reorganization happening at $P = 6-8$ GPa between PTM and the bridge. Gray lines show the

very small excess charge evolution under pressure for the two inequivalent molecules in the unit cell. These latter results indicate a slight tendency toward molecular charge order in the crystal.

In order to further verify that the here predicted crystal structures provide a realistic account of the radical dyad **1** under pressure, we compare high pressure Raman spectroscopy with spectra obtained from density functional theory calculations on these structures. The predicted crystalline structures, obtained with the above-described calculations, showing an increase of electronic bandwidths and the charge reorganization of dyad **1** under pressure provide a plausible explanation of the semiconducting behavior under the application of high pressure. However, a definitive confirmation of such crystalline structures by high-pressure XRD data is still pending.

**High-Pressure Raman Spectroscopy.** The Raman spectra of radical dyad **1** at different pressures were obtained using an excitation wavelength of 532 nm. This study has been complemented by calculation of the spectrum at different pressures based on the density functional theory (DFT) using a Gaussian basis set at the UM06/6-31G(d,p) level.[33,34] The spectra have been calculated for a single molecule whose structure has been extracted from the VASP optimized crystal structures at various pressures in the previous section. This

facilitates the Raman analysis by a detailed computational study on the assignment of the bands (see Figures S17–S19). In the 1700–1450 cm$^{-1}$ region, the bands at 1619 and 1597 cm$^{-1}$ are attributed to the C=C stretching modes of the benzene and vinylene units of the bridge, whereas the bands in the 1515–1480 cm$^{-1}$ region are mainly due to the C=C stretching of TTF and PTM moieties. The Raman spectra at selected pressures were recorded and their intensity was normalized with the band at 1515 cm$^{-1}$ (C=C stretching of TTF) (Figure S20a). On increasing the pressure, we observed that the Raman bands related to the bridge around 1600 cm$^{-1}$ progressively decreased in intensity. On the contrary, the bands assigned to the TTF and PTM units increased in intensity and overlapped when high-pressure was applied (Figure S20a). This tendency was also observed for the simulated Raman spectra obtained for the VASP predicted crystal structures at each applied pressure, confirming herewith the same behavior (Figure S20b). Moreover, the overlapping of the bands related to the TTF and PTM units suggests a change of the electronic delocalization on the molecule that could be related to the enhanced planarity of the molecules observed in the simulated crystal structures at high-pressures. On the other hand, in the region around 800 cm$^{-1}$, the bands attributed to the *out-of-plane* C–H bending broadened and decreased in intensity when increasing the pressure due to the fact that these vibrations were hindered because of the molecular packing.

We have performed a detailed analysis of the relative intensity variation of the measured Raman bands attributed to the vinylene bridge and those related to the PTM and TTF moieties along the entire pressure range to analyze possible phase transitions (Figure 9). We refer to the intensities as the
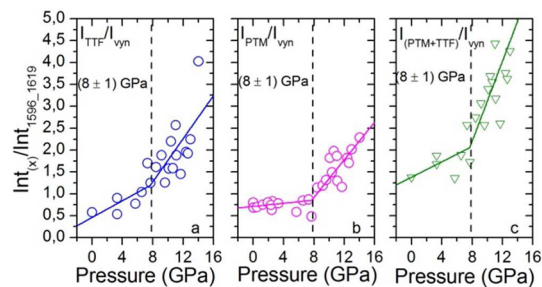


**Figure 9.** Intensity ratio of Raman bands of radical dyad **1** assigned to (a) C=C stretching of TTF/vinylene, (b) C=C stretching of PTM/vinylene bridge, and (c) C=C stretching of TTF+PTM/vinylene.

areas of Raman bands, calculating the sum of the areas of the bands at 1619 and 1597 cm$^{-1}$ for the vinylene bridge, the bands at 1570 and 1515 cm$^{-1}$ for the TTF and the bands at 1500 and 1486 cm$^{-1}$ for the PTM unit. We have calculated and plotted the intensity ratio for (*a*) the TTF stretching bands/vinylene bands, (*b*) the PTM stretching bands/vinylene bands, and (*c*) TTF+PTM bands/vinylene bands. A linear fit of the data shows two regions at pressures below and above 8 GPa with different slopes, with steeper slope at $P > 8$ GPa. These results suggest that while the system is reorganizing and readjusting the intermolecular spaces up to pressures of 8 GPa, the abrupt change of slope at 8 GPa indicates the presence of important intra- and intermolecular conformational changes that may originate from a crystalline phase transition. Note that our theoretical structure prediction does not show a true crystalline phase transition but rather a redistribution of electronic charge at about this pressure which is an indication that some

structural changes happened. The theoretical calculation may, for example, miss a structural phase transition because of the consideration of too small supercells for the relaxations. On the other hand, the evolution of these Raman bands is different from other PTM derivatives previously studied in our group[35] indicating a different electronic behavior for this system.

Apart from the changes in the relative intensities of the Raman bands, the most apparent effects of pressure on the Raman spectra are the upshifts of the spectral features with increasing pressure. This effect is analyzed in Figure S21 and Figure S22, where the frequencies of the most intense bands of PTM, vinylene bridge and TTF are plotted as a function of pressure. The observed shifts with pressure show a three regime stage where the different Raman bands shift with different slopes with increasing pressure. The three regimes would range from 0 to 2–5 GPa, from 2.5 to 8 GPa and, from 8 to 14 GPa (which is the highest pressure experimentally reached). The first regime is assigned to intermolecular rearrangements, since pressure barely induces any shifting of the bands. In the second one the bands show an important upshift with increasing pressure, indicating that pressure affects bonds and angles, which can be explained by conformational changes to readjust the electronic density. In the third regime, in general all analyzed bands show less steep slopes than in the intermediate regime but steeper than in the first regime. This indicates that pressures larger than 8 GPa must cause both intra- and intermolecular effects. These inter- and intramolecular pressure effects are confirmed by the reversibility observed in high pressure Raman experiments (Figure S23). Up to 1.6 GPa these changes are fully reversible, whereas from 6 GPa there are slight deviations between the relative intensities even though the spectral pattern remains. Finally, the recovered sample after compression of about 14.5 GPa is totally different from the pristine one.

**High-Pressure Photoluminescence Measurements.** In order to further investigate the intra- and intermolecular pressure effect observed by Raman spectroscopy, photo-luminescence measurements of crystals of radical dyad **1** when the sample was monochromatically excited with $\lambda = 532$ nm at different pressures were performed (Figure 10). High
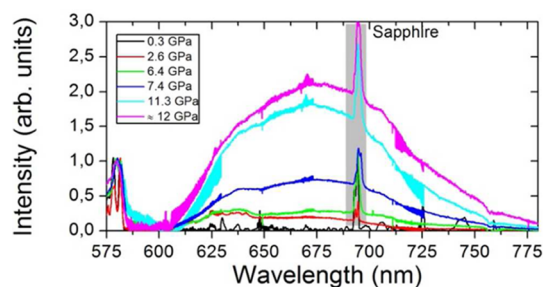


**Figure 10.** High resolution phtoluminescence spectra of crystals of radical dyad **1** at selected pressures when the sample was excited at 532 nm. The sample was supported on a nondrilled gold gasket and compressed using sapphire anvils with a 380 μm culet.

pressure experiments were conducted in a sapphire anvil cell and spectra were recorded at selected pressures up to 12 GPa. Whereas the pristine sample at 0 GPa does not show well-defined bands in the visible region, by increasing the pressure it is possible to observe the growth of a broad band in the 600–700 nm region (see Figure 9 and S24). This band that appears centered at 680 nm (1.8 eV) is much more intense when

increasing the pressure above 7 GPa as shown in Figure 10. The photophysical processes observed can be explained by the excitation of dyad **1** with light $\lambda = 532$ nm that induces a $264\alpha \rightarrow 266\alpha$ (SOMO $\rightarrow$ LUMO) electronic transition (see Supporting Information) as it has been already observed in similar systems.[36] At ambient pressure this electronic transition is practically forbidden, whereas by increasing the pressure the transition becomes more favored probably due to the enhanced electron delocalization and planarity of the system. Moreover, by increasing the pressure the intermolecular interactions become more important that could lead to an enhancement of the photoluminescence as it has been recently reported.[37,38] In order to analyze the reversibility of the photoluminescence properties at high pressure, we have measured the photo-luminescence spectrum of the recovered sample at 6 and 12 GPa (Figure S26). In both cases the intensity of the band remains the same indicating that conformational changes are not reversible and could be originated from a crystalline transition phase.

## ■ DISCUSSION

Analyzing all the experimental and theoretical studies, we can assume that the conductivity in radical dyad **1** between neighboring molecules takes place through the enhanced overlap between MPTTF and PTM under pressure. This overlap is absent in radical **2** which remains insulator at all considered pressures. When increasing the pressure, the electronic bandwidth $W$ in radical dyad **1** increases until it is able to offset the Coulomb repulsion $U$. In addition, simultaneous charge reorganization is happening that changes the charge on the radical subunits of dyad **1** molecules which are the units that contribute more to the electronic band (Figure 8c). In fact, band structure calculations above 8 GPa show that the gap between the bands dominated by TTF orbitals and the bands dominated by PTM orbitals disappear forming a wide band. Moreover, calculations of the evolution of charge transfer indicate that charge reorganization is taking place above the same applied pressures. On the other hand, high-pressure Raman spectroscopy supports this charge reorganization in a similar pressure regime and identical behavior was observed in the simulated spectra obtained for the VASP predicted crystal structures at each applied pressure. Reversibility studies on pressure-dependent Raman and photoluminescence measurements indicate that there is a change in the electronic conformation of the system in agreement with the enhanced planarity of the molecules and the intermolecular reorganization that could hint to a possible structural phase transition.

## ■ SUMMARY AND CONCLUSIONS

In summary, we have reported the observation of pressure induced conductivity in the nonplanar and spin localized neutral radical dyad **1** that exhibits a semiconductor behavior with high conductivity and low activation energy upon application of high pressure. In contrast, the model radical **2** remains as a Mott insulator under all applied pressures. This different behavior is due on the one hand to the supramolecular arrangement of molecules of **1** that permits to increase the bandwidth $W$ and as a consequence the $W/U$ ratio. Moreover, the reduction of the effective Coulomb interaction in **1** in comparison to **2** could be attributed to the enhanced electron delocalization in the system due to incorporation of a

substituent donor unit, as confirmed by Raman experiments and theoretical calculations. Overall we believe that the results described here are a proof of concept of a novel strategy providing an important insight into the design of new radical-based conductors. Thus, it may be possible to engineer radicals that can be conducting even without the need for applied pressure.

## ■ EXPERIMENTAL SECTION

**Synthesis and Characterization of Radicals 1 and 2.** The reagents and solvents used for synthesis and crystallization were of high purity grade (Sigma-Aldrich and SDS SA). Compounds **1** and compound **2** were prepared as previously reported in refs 27 and 39, respectively. The electrochemical experiments were performed with a potentiostat- galvanostast 263a (EG&G Princeton Applied Research) using platinum wires as counterelectrode and working electrode, a silver wire as reference electrode and as electrolyte a 0.1 M solution of tetrabutylammonium hexafluorophosphate (TBAHFP) in acetonitrile.

**Conductivity Measurements.** The four-probe resistivity measurements were performed with a Cryocooler helium compressor system (Sumitomo Heavy Industries, Ltd.). The KEITHLEY 224 Programmable current source and 182 Sensitive digital voltmeter were used for all measurements.

**Raman and Photoluminescence Measurements.** High pressure experiments were conducted in a sapphire anvil cell (SAC)[40,41] with a diameter culet of 360 $\mu$m and a gold gasket, specified in each section. No pressure transmitting medium was used and diamond chips were placed as the pressure calibrant. Raman and photoluminescence measurements were performed using an air-cooled argon ion laser, a Spectra-Physics solid state laser, operating at 532.0, nm. The device is equipped with a 10× Mitutoyo long working distance objective coupled to a 10× Navitar zoom system and focused onto the slit of an ISA HR460 monochromator with a grating of 600 grooves mm$^{-1}$ and a liquid nitrogen cooled CCD detector (ISA CCD3000, 1024−256 pixels). Spectra were measured with a spectral resolution of about 2−3 cm$^{-1}$ and calibrated with a standard neon emission lamp. The SAC is mounted on a xyz stage, which allows us to move the sample with an accuracy of 1 $\mu$m. The typical sampling area was about 1−2 $\mu$m in diameter. The simulated Raman spectra were calculated using the UM06 density functional theory[33] in conjunction with the 6-31G** basis set.[34]

**Theoretical Calculations.** Crystal structures at different pressures were simulated within density functional theory calculations[30] by performing relaxations of lattice parameters, monoclinic angle and internal atom positions at constant volume with the VASP code.[28,29] A plane wave cutoff of 400 eV was used as well as a $4 \times 4 \times 2$ k-mesh in the Brillouin zone. We checked, by performing enthalpy calculations that constant volume relaxations were of higher quality than constant pressure relaxations (not shown). All presented bulk electronic structure calculations were performed with the FPLO code[31] where a k-mesh of $6 \times 6 \times 6$ points was considered to converge the computations.

## ■ ASSOCIATED CONTENT

### ⓢ Supporting Information

The Supporting Information is available free of charge on the ACS Publications website at DOI: 10.1021/jacs.6b02888.

> Experimental details of X-ray crystallographic data and structure refinement. Simulated crystal structures of **1** at different pressures. Supplemental spectra of high-pressure conductivity, magnetic susceptibility, cyclic voltammetry, Raman and photoluminescence experiments. Simulated Raman spectra and details of theoretical calculations. (PDF)
> Crystal data. (CIF)
> Crystal data. (CIF)
> Crystal data. (CIF)

## AUTHOR INFORMATION

### Corresponding Author
*vecianaj@icmab.es

### Notes
The authors declare no competing financial interest.

## REFERENCES

(1) Rovira, C. Chem. Rev. 2004, 104, 5289.
(2) Farges, J. P. Organic Conductors: Fundamentals and Applications; Marcel Dekker: New York, 1994.
(3) Bndikov, M.; Wudl, F.; Perepichka, D. F. Chem. Rev. 2004, 104, 4891.
(4) Nunes, J. P. M.; Figueira, M. J.; Belo, D.; Santos, I. C.; Ribeiro, B.; Lopes, E. B.; Henriques, R. T.; Vidal-Gancedo, J.; Veciana, J.; Rovira, C.; Almeida, M. Chem. - Eur. J. 2007, 13, 9841.
(5) Tanaka, H.; Okano, Y.; Kobayashi, H.; Suzuki, W.; Kobayashi, A. Science 2001, 291, 285.
(6) Cui, H.; Kobayashi, H.; Ishibashi, S.; Sasa, M.; Iwase, F.; Kato, R.; Kobayashi, A. J. Am. Chem. Soc. 2014, 136, 7619.
(7) Jerome, D.; Mazaud, A.; Ribault, M.; Bechgaard, K. J. Phys., Lett. 1980, 31, 95.
(8) Haddon, R. C. Nature 1975, 256, 394.
(9) Chi, X.; Itkis, M. E.; Reed, R. W.; Oakley, R. T.; Cordes, A. W.; Haddon, R. C. J. Phys. Chem. B 2002, 106, 8278.
(10) Pal, S. K.; Itkis, M. E.; Tham, F. S.; Reed, R. W.; Oakley, R. T.; Haddon, R. C. Science 2005, 309, 281.
(11) Pal, S. K.; Itkis, M. E.; Tham, F. S.; Reed, R. W.; Oakley, R. T.; Donnadieu, B.; Haddon, R. C. J. Am. Chem. Soc. 2007, 129, 7163.
(12) Haddon, R. C.; Sarkar, A.; Pal, S. K.; Chi, X.; Itkis, M. E.; Tham, F. S. J. Am. Chem. Soc. 2008, 130, 13683.
(13) Pal, S. K.; Itkis, M. E.; Tham, F. S.; Reed, R. W.; Oakley, R. T.; Haddon, R. C. J. Am. Chem. Soc. 2008, 130, 3942.
(14) Pal, S. K.; Bag, P.; Sarkar, A.; Chi, X.; Itkis, M. E.; Tham, F. S.; Donnadieu, B.; Haddon, R. C. J. Am. Chem. Soc. 2010, 132, 17258.
(15) Sarkar, A.; Itkis, M. E.; Tham, F. S.; Haddon, R. C. Chem. - Eur. J. 2011, 17, 11576.
(16) Bag, P.; Itkis, M. E.; Pal, S. K.; Bekyarova, E.; Donnadieu, B.; Haddon, R. C. J. Phys. Org. Chem. 2012, 25, 566.

(17) Pal, S. K.; Bag, P.; Itkis, M. E.; Tham, F. S.; Haddon, R. C. J. Am. Chem. Soc. 2014, 136, 14738.
(18) Brusso, J. L.; Cvrkalj, K.; Leitch, A.; Oakley, R. T.; Reed, R. W.; Robertson, C. M. J. Am. Chem. Soc. 2006, 128, 15080.
(19) Mailman, A.; Winter, S. M.; Yu, X.; Robertson, C. M.; Yong, W.; Tse, J. S.; Secco, R. A.; Liu, X.; Dube, P. A.; Howard, J. A. K.; Oakley, R. T. J. Am. Chem. Soc. 2012, 134, 9886.
(20) Yu, X.; Mailman, A.; Lekin, K.; Assoud, A.; Robertson, C. M.; Noll, B. C.; Campana, C. F.; Howard, J. A. K.; Dube, P. A.; Oakley, R. T. J. Am. Chem. Soc. 2012, 134, 2264.
(21) Leitch, A. A.; Lekin, K.; Winter, S. M.; Downie, L. E.; Tsuruda, H.; Tsell, J. S.; Mito, M.; Desgreniers, S.; Dube, P. A.; Zhang, S.; Liu, Q.; Jin, C.; Ohishi, Y.; Oakley, R. T. J. Am. Chem. Soc. 2011, 133, 6051.
(22) Wong, J. W. L.; Mailman, A.; Lekin, K.; Winter, S. M.; Yong, W.; Zhao, J.; Garimella, S. V.; Tse, J. S.; Secco, R. A.; Desgreniers, S.; Ohishi, Y.; Borondics, F.; Oakley, R. T. J. Am. Chem. Soc. 2014, 136, 1070.
(23) Ratera, I.; Veciana, J. Chem. Soc. Rev. 2012, 41, 303.
(24) Guasch, J.; Grisanti, L.; Lloveras, V.; Vidal-Gancedo, J.; Souto, M.; Morales, D. C.; Vilaseca, M.; Sissa, C.; Painelli, A.; Ratera, I.; Rovira, C.; Veciana, J. Angew. Chem., Int. Ed. 2012, 51, 11024.
(25) Guasch, J.; Grisanti, L.; Souto, M.; Lloveras, V.; Vidal-Gancedo, J.; Ratera, I.; Painelli, A.; Rovira, C.; Veciana, J. J. Am. Chem. Soc. 2013, 135, 6958.
(26) Souto, M.; Guasch, J.; Lloveras, V.; Mayorga, P.; López-Navarrete, J. T.; Casado, J.; Ratera, I.; Rovira, C.; Painelli, A.; Veciana, J. J. Phys. Chem. Lett. 2013, 4, 2721.
(27) Souto, M.; Solano, M. V.; Jensen, M.; Bendixen, D.; Delchiaro, F.; Girlando, A.; Painelli, A.; Jeppesen, J. O.; Rovira, C.; Ratera, I.; Veciana, J. Chem. - Eur. J. 2015, 21, 8816.
(28) Kresse, G.; Hafner, J. Phys. Rev. B: Condens. Matter Mater. Phys. 1993, 47, 558.
(29) Kresse, G.; Furthmüller, J. Phys. Rev. B: Condens. Matter Mater. Phys. 1996, 54, 11169.
(30) Perdew, J. P.; Burke, K.; Ernzerhof, M. Phys. Rev. Lett. 1996, 77, 3865.
(31) Koepernik, K.; Eschrig, H. Phys. Rev. B: Condens. Matter Mater. Phys. 1999, 59, 1743.
(32) Kotliar, G.; Vollhardt, D. Phys. Today 2004, 57, 53.
(33) Zhao, Y.; Truhlar, D. G. Theor. Chem. Acc. 2006, 120, 215.
(34) Frisch, M. J.; Trucks, G. W.; Schlegel, H. B.; Scuseria, G. E.; Robb, M. A.; Cheeseman, J. R.; Scalmani, G.; Barone, V.; Mennucci, B.; Petersson, G. A.; Nakatsuji, H.; Caricato, M.; Li, X.; Hratchian, H. P.; Izmaylov, A. F.; Bloino, J.; Zheng, G.; Sonnenberg, J. L.; Hada, M.; Ehara, M.; Toyota, K.; Fukuda, R.; Hasegawa, J.; Ishida, M.; Nakajima, T.; Honda, Y.; Kitao, O.; Nakai, H.; Vreven, T.; Montgomery, J. A., Jr.; Peralta, J. E.; Ogliaro, F.; Bearpark, M.; Heyd, J. J.; Brothers, E.; Kudin, K. N.; Staroverov, V. N.; Kobayashi, R.; Normand, J.; Raghavachari, K.; Rendell, A.; Burant, J. C.; Iyengar, S. S.; Tomasi, J.; Cossi, M.; Rega, N.; Millam, J. M.; Klene, M.; Knox, J. E.; Cross, J. B.; Bakken, V.; Adamo, C.; Jaramillo, J.; Gomperts, R.; Stratmann, R. E.; Yazyev, O.; Austin, A. J.; Cammi, R.; Pomelli, C.; Ochterski, J. W.; Martin, R. L.; Morokuma, K.; Zakrzewski, V. G.; Voth, G. A.; Salvador, P.; Dannenberg, J. J.; Dapprich, S.; Daniels, A. D.; Farkas, O.; Foresman, J. B.; Ortiz, J. V.; Cioslowski, J.; Fox, D. J. Gaussian 09, Revision A.02; Gaussian, Inc.: Wallingford, CT, 2009.
(35) Rodríguez, S.; Nieto-Ortega, B.; González-Cano, R. C.; Lloveras, V.; Novoa, J. J.; Mota, F.; Vidal-Gancedo, J.; Rovira, C.; Veciana, J.; Del Corro, E.; Taravillo, M.; Baonza, V. G.; López-Navarrete, J. T.; Casado, J. J. Chem. Phys. 2014, 140, 164903/1−164903/9.
(36) Hattori, Y.; Kusamoto, T.; Nishihara, H. Angew. Chem., Int. Ed. 2014, 53, 11845.
(37) Yuan, H.; Wang, K.; Yang, K.; Liu, B.; Zou, B. J. Phys. Chem. Lett. 2014, 5, 2968.
(38) Schmidtke, J. P.; Kim, J.-S.; Gierschner, J.; Silva, C.; Friend, R. H. Phys. Rev. Lett. 2007, 99, 167401.
(39) Armet, O.; Veciana, J.; Rovira, C.; Riera, J.; Castañer, J.; Molins, E.; Rius, J.; Miravitlles, C.; Olivella, S.; Brichfeus, J. J. Phys. Chem. 1987, 91, 5608.

(40) Baonza, V. G.; Taravillo, M.; Arencibia, A.; Cáceres, M.; Núñez, J. *J. Raman Spectrosc.* **2003**, *34*, 264.

(41) Del Corro, E.; González, J.; Taravillo, M.; Flahaut, E.; Baonza, V. G. *Nano Lett.* **2008**, *8*, 2215.